

Polar methane accumulation and rainstorms on Titan from simulations of the methane cycle

T. Schneider¹, S. D. B. Graves¹, E. L. Schaller² & M. E. Brown¹

Titan has a methane cycle akin to Earth's water cycle. It has lakes in polar regions^{1,2}, preferentially in the north³; dry low latitudes with fluvial features^{4,5} and occasional rainstorms^{6,7}; and tropospheric clouds mainly (so far) in southern middle latitudes and polar regions^{8–15}. Previous models have explained the low-latitude dryness as a result of atmospheric methane transport into middle and high latitudes¹⁶. Hitherto, no model has explained why lakes are found only in polar regions and preferentially in the north; how low-latitude rainstorms arise; or why clouds cluster in southern middle and high latitudes. Here we report simulations with a three-dimensional atmospheric model coupled to a dynamic surface reservoir of methane. We find that methane is cold-trapped and accumulates in polar regions, preferentially in the north because the northern summer, at aphelion, is longer and has greater net precipitation than the southern summer. The net precipitation in polar regions is balanced in the annual mean by slow along-surface methane transport towards mid-latitudes, and subsequent evaporation. In low latitudes, rare but intense storms occur around the equinoxes, producing enough precipitation to carve surface features. Tropospheric clouds form primarily in middle and high latitudes of the summer hemisphere, which until recently has been the southern hemisphere. We predict that in the northern polar region, prominent clouds will form within about two (Earth) years and lake levels will rise over the next fifteen years.

Explanations for Titan's tropospheric clouds range from control by local topography and cryovolcanism^{11,12} to control by a seasonally varying global Hadley circulation with methane condensation in its ascending branch^{8,17}. General circulation models (GCMs) have suggested that clouds either form primarily in mid-latitudes and near the poles in both hemispheres¹⁸—which is inconsistent with the observed hemispheric differences¹⁴—or that they form where insolation is at a maximum¹⁷, which is likewise not fully consistent with newer observations^{14,15}. Similarly, explanations for the polar hydrocarbon lakes range from control by local topography and a subsurface methane table² to control by evaporation and precipitation, which depend on the atmospheric circulation^{16,19}. GCMs have suggested that surface methane accumulates near the poles, but also show it in mid-latitudes¹⁶, where no lakes have been observed, and they have failed to reproduce the observed hemispheric asymmetry. Additionally, no model is fully consistent with the cloud distribution or has shown low-latitude precipitation that is intense enough to carve fluvial features. Indeed, it has been suggested that the atmosphere is too stable for rainstorms to occur in low latitudes²⁰. Yet intense and, in at least one case, apparently precipitating storms have been observed^{6,7}.

To investigate the extent to which major features of Titan's climate and methane cycle can be explained by large-scale processes, we use a GCM that includes an atmospheric model with a methane cycle and surface reservoir. The atmospheric model is three-dimensional (3D), in contrast to previous two-dimensional (2D) models^{16–18}, because the intermittency of clouds and features such as equatorial super-rotation²¹ (impossible in axisymmetric circulations²²) point to the importance of 3D dynamics. The surface reservoir gains or loses methane according to

the local rates of precipitation (P) and evaporation (E), with horizontal diffusion as a simple representation of slow surface flows from moister to drier regions. We show zonal and temporal averages from a simulation in a statistically steady state, which does not depend on initial conditions except for the (conserved) total methane amount present in the atmosphere-surface system (here, the equivalent of 12 m liquid methane in the global mean if all methane were condensed at the surface). See Supplementary Information for details.

In the statistically steady state, our model shows an annual- and global-mean methane concentration in the atmosphere corresponding to 7 m liquid methane—possibly higher than, but broadly consistent with, observations^{23,24}. The remainder is at the surface. Methane has accumulated near the poles (Fig. 1a). It is transported there from spring into summer by a global Hadley circulation (Fig. 1b), with ascent (Fig. 2) and a precipitation maximum (Fig. 1c) over the summer pole. Some of the methane accumulating near the summer pole flows along the surface (on Titan it may also flow beneath the surface²) towards mid-latitudes. It evaporates and is transported back towards the opposite pole when the circulation reverses, around equinox. Polar regions lose methane from late summer to winter, with zonal-mean net evaporation rates ($E - P$) reaching around 0.2 m yr^{-1} (1 yr referring to 1 Earth year) in the southern summer (Fig. 1b). This is consistent with observations: the zonal-mean evaporative loss rate is of similar magnitude to (but smaller than) the recently observed local drop in south-polar lake levels²⁵. We predict that the north-polar region will gain methane for roughly the next 15 yr, with zonal-mean net precipitation rates ($P - E$) reaching about 1.4 m yr^{-1} around the northern summer solstice (NSS; Fig. 1b). This should lead to an observable rise in lake levels.

Methane is cold-trapped at the poles. Along with annual-mean insolation, annual-mean evaporation is at its lowest near the poles. (Evaporation is the dominant loss term in the surface energy balance and scales with insolation.) Surface temperatures decrease from low latitudes towards the poles throughout the year (Fig. 1d), because almost all solar energy absorbed at the poles is used to evaporate methane. At the same time, precipitation is highest near the summer pole (Fig. 1c) because the insolation maximum destabilizes the atmosphere with respect to moist convection. This can be seen from the moist static energy (MSE), which is a more direct measure than temperature for the energetic effect of solar radiation on the atmosphere. This is because if, as on Titan and in our GCM, the surface heat capacity is negligible²⁶, only net radiation at the top of the atmosphere drives the vertically integrated MSE balance; similarly, insolation variations are the dominant driver of variations in the MSE balance integrated over the planetary boundary layer. Indeed, along with insolation, near-surface MSE is highest near the summer poles (Fig. 1e). This implies a propensity for deep convection, because the slow rotation and large thermal inertia of Titan's atmosphere constrain horizontal and temporal variations in temperature and MSE above the boundary layer, keeping them weak²⁷, and the vertical MSE stratification controls convective stability (MSE increasing with altitude indicates stability; ref. 26). Lower latitudes, by contrast, do not favour deep

¹California Institute of Technology, Pasadena, California 91125, USA. ²NASA Dryden Aircraft Operations Facility, National Suborbital Education and Research Center, Palmdale, California 93550, USA.

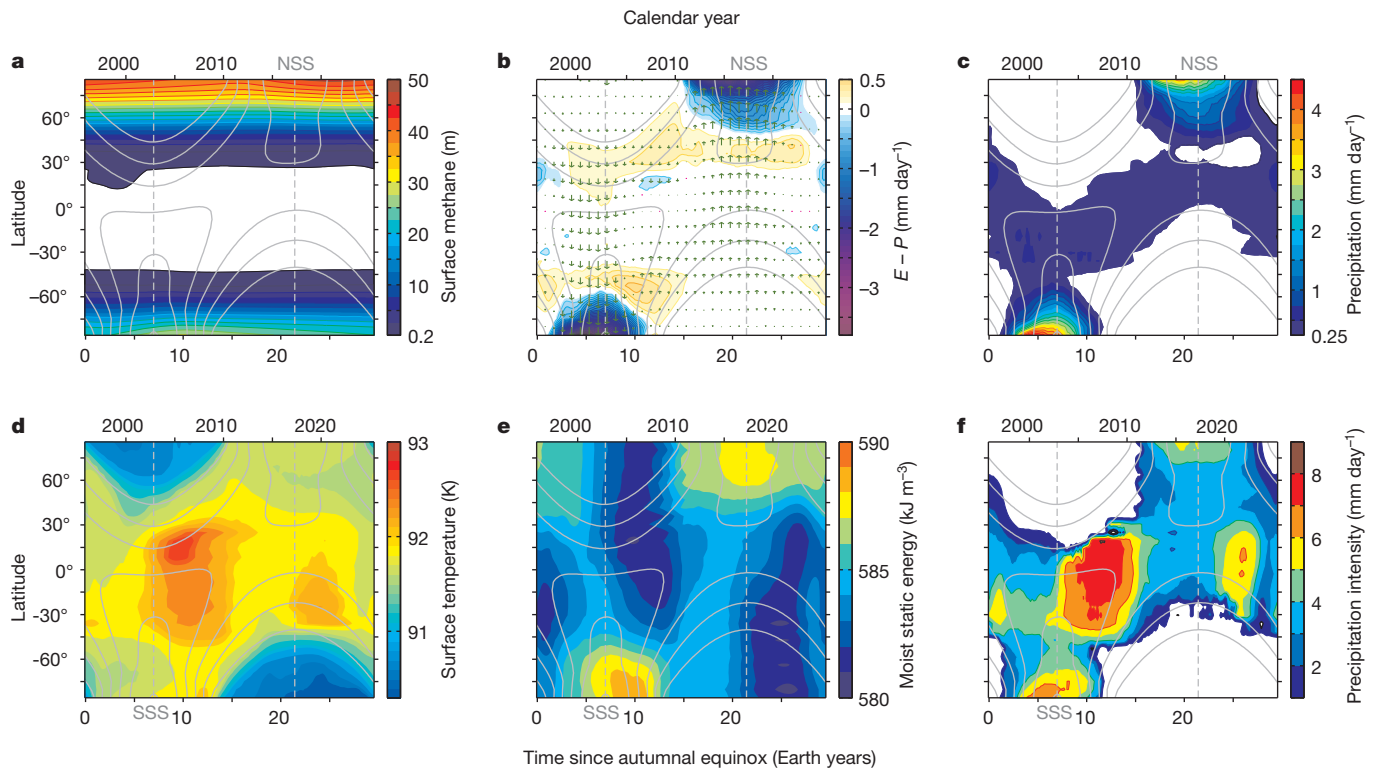


Figure 1 | Annual cycle of zonal-mean climate statistics in Titan GCM. The lower time axes start at the autumnal equinox (corresponding to November 1995); the upper axes indicate corresponding calendar years. Solid grey lines are contours of absorbed solar radiation at the surface (contour interval 0.25 W m^{-2}), and dashed grey lines mark the northern summer solstice (NSS) and southern summer solstice (SSS). **a**, Methane surface-reservoir depth (colour scale truncated at 20 cm). **b**, Net evaporation ($E - P$) at the surface (colours, contour interval 0.1 mm day^{-1} , with 1 day = 86,400 s) and column-integrated meridional methane flux (arrows, with the longest corresponding to a flux of $5.4 \text{ kg m}^{-1} \text{ s}^{-1}$). The methane flux is largely accomplished by the mean meridional (Hadley) circulation; eddy fluxes are weaker by a factor of 3 or larger, and are strongest in the middle and low latitudes. **c**, Precipitation rate. **d**, Surface temperature. The surface temperatures are roughly consistent with observations³⁰, with similar equator–pole temperature contrasts and with a

convection, even though they are warmer than the summer poles, because their maximum insolation is weaker, so their maximum near-surface MSE is also lower (Fig. 1e). The result is the drying of lower latitudes and the accumulation of methane at the poles, similar to the results of previous models but without methane accumulation in mid-latitudes¹⁶ (see Supplementary Information for possible reasons for this difference).

In the model's low latitudes, rainstorms are rare but intense: that is, although low latitudes are dry and have smaller mean precipitation rates than the poles (Fig. 1c), they have the largest precipitation intensity (Fig. 1f). Precipitation rates in the more intense storms are greater than 10 mm per (Earth) day, similar to rough estimates of the rates needed to carve the observed fluvial surface features^{4,28}. The precipitation intensity is largest before and around the equinoxes, when the reversal of the Hadley circulation (see Fig. 1b) is associated with dynamic instabilities. These instabilities generate waves strong enough to trigger deep convection and intense rain if they advect relatively moist air from higher latitudes over the warm low latitudes. This is in contrast to 2D and local models that suggest that intense precipitation does not occur in low latitudes^{16–18,20}, however, it is consistent with the observations of intense and apparently precipitating low-latitude storms on Titan^{6,7}.

In the GCM as on Titan³, there is more surface methane in the northern polar regions than in the southern (Fig. 1a). This asymmetry is a consistent feature, irrespective of initial conditions (for example, whether methane is initially in the atmosphere or at the surface). It is

winter pole that is around 1 K colder than the summer pole. (Generally, tropospheric temperatures in the simulation are within 1 K of Titan observations; see Supplementary Fig. 2.) **e**, MSE per unit volume averaged between surface and 2-km altitude. MSE is the sum of gravitational potential energy and moist enthalpy, including the contribution of the latent heat of methane vapour²⁶. **f**, Precipitation intensity (precipitation rate when it rains). The precipitation intensity is the mean precipitation conditional on the precipitation rate being non-zero (exceeding $10^{-3} \text{ mm day}^{-1}$). All fields are averages over longitude and time (25 Titan yr) in the statistically steady state of a simulation with a total of 12 m liquid methane in the atmosphere–surface system. The statistically steady state was reached over a long (135 Titan yr) spin-up period. Although the GCM climate is statistically zonally symmetric, climate statistics such as the methane surface-reservoir depth exhibit instantaneous zonal asymmetries ('lakes'), which can persist for several Titan years.

caused by Saturn's orbital eccentricity, which leads to a northern summer (currently around aphelion) that is longer and cooler than the southern, and therefore allows more methane to be cold-trapped. Although the maximum rate of net precipitation (Fig. 1b) is greatest in the warmer southern summer, polar net precipitation integrated over a Titan year (about 30 Earth years) is greatest in the north, primarily because its rainy season is longer. For example, averaged over the polar caps bounded by the polar circles (63.3° N/S), the period during which absorbed insolation exceeds 0.5 W m^{-2} is 14% longer in the north than in the south. Annually integrated net precipitation is 0.86 m (38%) greater in the north; 0.76 m of this is attributable to increased precipitation, and 0.10 m to decreased evaporation. (The contribution of evaporation to the hemispheric asymmetry is small because it scales with insolation, which, in the annual mean, is equal in the north and south; this contradicts a previous hypothesis that the hemispheric asymmetry is due to evaporation differences³.) In the model's annual mean, the excess net precipitation in polar regions is balanced by along-surface methane transport towards mid-latitudes and subsequent evaporation, so surface methane extends farther towards the equator in the north than in the south (Fig. 1a). The same is true on Titan³. Thus, surface or sub-surface transport of methane is essential for maintaining a statistically steady state with non-zero net precipitation in polar regions and asymmetries between the hemispheres; we expect that such transport occurs on Titan. One reason that previous models¹⁶ did not produce hemispheric asymmetries is that they were lacking a representation of this transport.

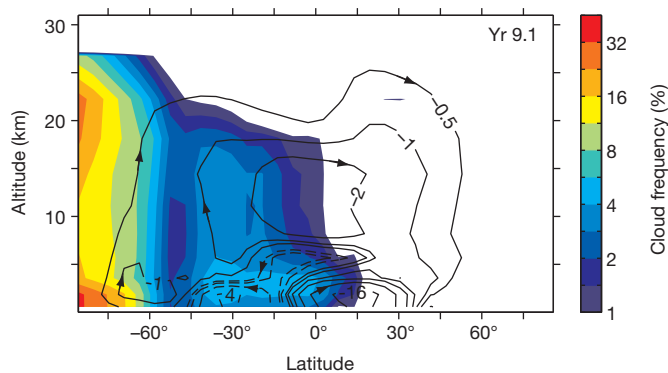


Figure 2 | Relationship between tropospheric cloudiness and atmospheric circulation in southern summer in Titan GCM. Colours show the tropospheric methane-cloud frequency and contours show the stream function of the mean meridional mass circulation, both at 9.1 yr past autumnal equinox (corresponding to January 2005, the time of the Huygens landing on Titan). The contouring is logarithmic, with factors of $\sqrt{2}$ and 2 between adjacent contour levels for cloud frequency and stream function, respectively. Solid stream-function contours for clockwise rotation, dashed contours for anticlockwise rotation (contour levels at $\pm 2^{-1}, 1, 2^2, \dots \times 10^9 \text{ kg s}^{-1}$). The cloud frequency is the relative frequency of phase changes of methane on the grid scale and in the convection scheme of the GCM. Moist convection and maxima in cloud frequency above the boundary layer occur above the polar near-surface MSE maximum and above relatively high surface temperatures in mid-latitudes (here, at around 30°S) in the summer hemisphere. (Moist convection rarely occurs above the local surface-temperature maximum in the winter hemisphere (here, at $15^\circ\text{--}30^\circ \text{N}$), because this lies under the descending branch of the Hadley circulation, where the free troposphere is relatively dry.)

Our GCM also reproduces the observed tropospheric methane-cloud distribution (Fig. 3). For the period with detailed observations (2001 onwards), the GCM reproduces the observed prevalence of clouds in the southern hemisphere mid-latitudes and polar region; it also reproduces the decreasing frequency of south-polar clouds since 2005 (Fig. 3a)^{6,13–15}. For 2001 onwards, the GCM indicates a lack of clouds in the northern hemisphere, consistent with observations of Titan made with ground-based telescopes^{6,13} and the Cassini Visual and Infrared Mapping Spectrometer (VIMS; ref. 14). Observations with the Cassini Imaging Science Subsystem (ISS; ref. 15) indicate more frequent northern-hemisphere clouds (Fig. 3a), but these seem to be lake-effect clouds: they are associated with stationary zonal inhomogeneities in topography and the lake distribution²⁹ that are not captured in the GCM. The relative frequency of clouds in the GCM fits observations better than previous 2D models^{16–18}. A 3D model that resolves waves and instabilities in the atmosphere is essential for reproducing the non-sinusoidal seasonal variations of cloudiness.

Deep convective clouds in the GCM form not only above the polar near-surface MSE maximum, but also in the summer-hemisphere mid-latitudes (Fig. 2). There they form above relatively high surface temperatures (Fig. 1d), which destabilize the boundary layer with respect to dry convection. This occasionally leads to moist convection and mean ascent in the free troposphere (above shallow boundary-layer circulation cells), resulting in a secondary cloud-frequency maximum above the boundary layer (Fig. 2). The surface reservoir underneath these clouds is depleted (less than 7 cm depth in the mean, see Fig. 1a), consistent with the observed lack of lakes in mid-latitudes². We predict that, with the reversal of the Hadley circulation in spring, north-polar clouds will emerge within about 2 yr, earlier than suggested by other models¹⁷, and should be clearly observable for roughly 10 yr; around NSS, prominent cloudiness may extend into mid-latitudes (Fig. 3b). The validity of our predictions of seasonal changes will soon be testable as Titan's northern-hemisphere spring proceeds into summer and new observations become available.

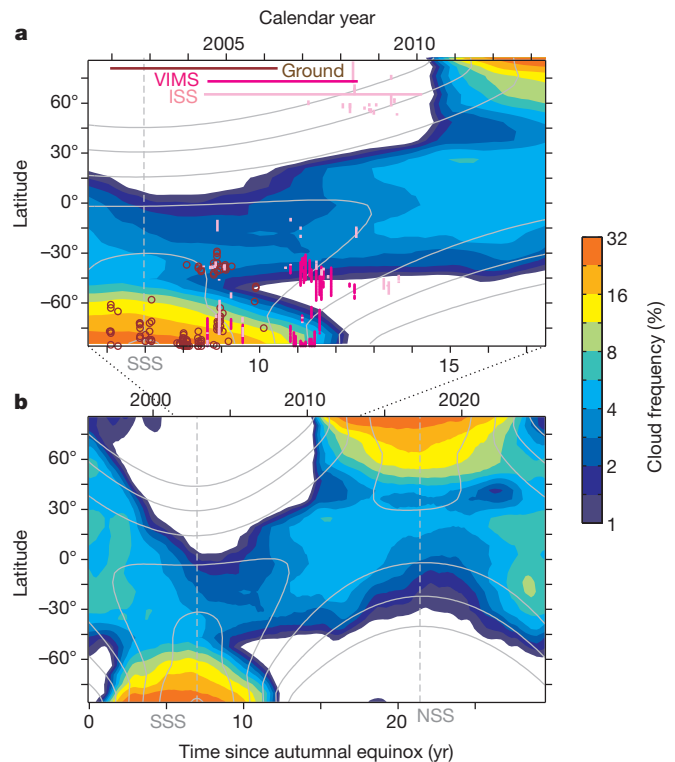


Figure 3 | Annual cycle of tropospheric methane-cloud frequency. **a**, Cloud frequency in GCM and cloud observations, focusing on the time period for which detailed observations are available or will be available soon. The GCM cloud frequency (Fig. 2) in the troposphere between the surface and 32-km altitude. Brown circles, ground-based cloud observations¹³; magenta lines, Cassini VIMS observations¹⁴; light pink lines, Cassini ISS observations¹⁵. The bars across the top indicate the time period over which the observations were made. (However, the coverage of VIMS and ISS observations is not continuous, so a lack of VIMS and ISS cloud observations in the periods indicated by the bars does not necessarily mean clouds were in fact absent.) Solid grey lines, contours of absorbed solar radiation at the surface, as in Fig. 1. **b**, As in **a**, except over a complete Titan year, beginning at autumnal equinox, and excluding observations.

Received 4 August; accepted 20 October 2011.

1. Stofan, E. *et al.* The lakes of Titan. *Nature* **445**, 61–64 (2007).
2. Hayes, A. *et al.* Hydrocarbon lakes on Titan: distribution and interaction with a porous regolith. *Geophys. Res. Lett.* **35**, L09204 (2008).
3. Aharonson, O. *et al.* An asymmetric distribution of lakes on Titan as a possible consequence of orbital forcing. *Nature Geosci.* **2**, 851–854 (2009).
4. Lebreton, J. *et al.* An overview of the descent and landing of the Huygens probe on Titan. *Nature* **438**, 758–764 (2005).
5. Lorenz, R. *et al.* The sand seas of Titan: Cassini RADAR observations of longitudinal dunes. *Science* **312**, 724–727 (2006).
6. Schaller, E. L., Roe, H. G., Schneider, T. & Brown, M. E. Storms in the tropics of Titan. *Nature* **460**, 873–875 (2009).
7. Turtle, E. P. *et al.* Rapid and extensive surface changes near Titan's equator: evidence of April showers. *Science* **331**, 1414–1417 (2011).
8. Brown, M. E., Bouchez, A. H. & Griffith, C. A. Direct detection of variable tropospheric clouds near Titan's south pole. *Nature* **420**, 795–797 (2002).
9. Porco, C. C. *et al.* Imaging of Titan from the Cassini spacecraft. *Nature* **434**, 159–168 (2005).
10. Griffith, C. A. *et al.* The evolution of Titan's mid-latitude clouds. *Science* **310**, 474–477 (2005).
11. Roe, H. G., Bouchez, A. H., Trujillo, C. A., Schaller, E. L. & Brown, M. E. Discovery of temperate latitude clouds on Titan. *Astrophys. J.* **618**, L49–L52 (2005).
12. Roe, H. G., Brown, M. E., Schaller, E. L., Bouchez, A. H. & Trujillo, C. A. Geographic control of Titan's mid-latitude clouds. *Science* **310**, 477–479 (2005).
13. Schaller, E. L., Brown, M. E., Roe, H. G., Bouchez, A. H. & Trujillo, C. A. Dissipation of Titan's south polar clouds. *Icarus* **184**, 517–523 (2006).
14. Brown, M. E., Roberts, J. E. & Schaller, E. L. Clouds on Titan during the Cassini prime mission: A complete analysis of the VIMS data. *Icarus* **205**, 571–580 (2010).
15. Turtle, E. P. *et al.* Seasonal changes in Titan's meteorology. *Geophys. Res. Lett.* **38**, L03203 (2011).
16. Mitchell, J. The drying of Titan's dunes: Titan's methane hydrology and its impact on atmospheric circulation. *J. Geophys. Res.* **113**, E08015 (2008).

17. Mitchell, J. L., Pierrehumbert, R. T., Frierson, D. M. W. & Caballero, R. The dynamics behind Titan's methane clouds. *Proc. Natl Acad. Sci. USA* **103**, 18421–18426 (2006).
18. Rannou, P., Montmessin, F., Hourdin, F. & Lebonnois, S. The latitudinal distribution of clouds on Titan. *Science* **311**, 201–205 (2006).
19. Mitri, G., Showman, A. P., Lunine, J. I. & Lorenz, R. D. Hydrocarbon lakes on Titan. *Icarus* **186**, 385–394 (2007).
20. Griffith, C. A., McKay, C. P. & Ferri, F. Titan's tropical storms in an evolving atmosphere. *Astrophys. J.* **687**, L41–L44 (2008).
21. Flasar, F. M., Baines, K. H., Bird, M. K., Tokano, T. & West, R. A. Atmospheric dynamics and meteorology. In Brown, R. H., Lebreton, J. P. & Waite, J. H. (eds) *Titan from Cassini-Huygens* Chap. 13, 323–352 (Springer, 2009).
22. Schneider, T. The general circulation of the atmosphere. *Annu. Rev. Earth Planet. Sci.* **34**, 655–688 (2006).
23. Penteado, P. F., Griffith, C. A., Greathouse, T. K. & de Bergh, C. Measurements of CH₃D and CH₄ in Titan from infrared spectroscopy. *Astrophys. J.* **629**, L53–L56 (2005).
24. Tokano, T. *et al.* Methane drizzle on Titan. *Nature* **442**, 432–435 (2006).
25. Hayes, A. *et al.* Transient surface liquid in Titan's polar regions from Cassini. *Icarus* **211**, 655–671 (2011).
26. Neelin, J. D. & Held, I. M. Modeling tropical convergence based on the moist static energy budget. *Mon. Weath. Rev.* **115**, 3–12 (1987).
27. Charney, J. G. A note on large-scale motions in the tropics. *J. Atmos. Sci.* **20**, 607–609 (1963).
28. Perron, J. T. *et al.* Valley formation and methane precipitation rates on Titan. *J. Geophys. Res.* **111**, E11001 (2006).
29. Brown, M. E. *et al.* Discovery of lake-effect clouds on Titan. *Geophys. Res. Lett.* **36**, L01103 (2009).
30. Jennings, D. E. *et al.* Titan's surface brightness temperatures. *Astrophys. J.* **691**, L103–L105 (2009).

Supplementary Information is linked to the online version of the paper at www.nature.com/nature.

Acknowledgements We are grateful for support by a NASA Earth and Space Science Fellowship and a David and Lucile Packard Fellowship. We thank I. Eisenman for code for the insolation calculations, and O. Aharonson, A. Hayes and A. Soto for comments on a draft. The simulations were done on the California Institute of Technology's Division of Geological and Planetary Sciences Dell cluster.

Author Contributions T.S. and M.E.B. conceived the study; T.S., S.D.B.G. and E.L.S. developed the GCM; E.L.S. and M.E.B. provided data; and T.S. and S.D.B.G. wrote the paper, with contributions and comments from all authors.

Author Information Reprints and permissions information is available at www.nature.com/reprints. The authors declare no competing financial interests. Readers are welcome to comment on the online version of this article at www.nature.com/nature. Correspondence and requests for materials should be addressed to T.S. (tapio@caltech.edu).